Effects of Synthetic Amphiphilic α-Helical Peptides on the Electrochemical and Structural Properties of Supported Hybrid Bilayers on Gold

Matthew B. Smith, Jihong Tong, Jan Genzer, Daniel Fischer, and Peter K. Kilpatrick*

Department of Chemical and Biomolecular Engineering, North Carolina State University, Box 7905, Raleigh, North Carolina 27695-7905

Received April 25, 2005. In Final Form: November 2, 2005

Amphiphilic α-helices were formed from designed synthetic peptides comprising alanine, phenylalanine, and lysine residues. The insertion of the α-helical peptides into hybrid bilayers assembled on gold was studied by a variety of methods to assess the resulting structural characteristics, such as electrical resistance and molecular orientation. Self-assembled monolayers (SAMs) of dodecanethiol (DDT); octadecanethiol (ODT); and 1,2-dipalmitoyl-*sn*-glycero-3-phosphothioethanol (DPPTE) were formed on gold substrates with and without incorporated peptide. Supported hybrid bilayers and multilayers of 1,2-dimyristoyl-*sn*-glycero-3-phosphocholine (DMPC) were formed on SAMs by the "paint-freeze" method of bilayer formation. Modeling of electrochemical impedance spectroscopy data using equivalent electrochemical circuits revealed that the addition of peptide decreased dramatically the resistive element of the bilayer films while maintaining the value of the capacitive element, indicating successful incorporation of peptide into a well-formed bilayer. Near-edge X-ray absorption fine structure spectroscopy data provided evidence that the molecules in the SAMs and hybrid multilayers were ordered even in the presence of peptide. The peptide insertion into the SAM was confirmed by observing the π^* resonance peak correlating with phenylalanine and a peak in the nitrogen K-edge regime attributable to the peptide bond.

Introduction

Solid-supported organic monolayers and lipid bilayers on noble metals have emerged as important research tools in recent years. Solid-supported membranes on flat substrates represent useful analogues to cellular membranes for protein research because of their high structural integrity and the variety of methods that can be applied to probe their properties. There is great interest in utilizing these systems as elements of biosensors as well as in the study of transmembrane peptide interactions with biomimetic films.[1−10] Furthermore, supported lipid-bilayers on solid metal substrates may be readily characterized using electrical techniques such as electrochemical impedance spectroscopy and cyclic voltammetry.[3,11−17] Our efforts focus on studying and understanding the conditions under which synthetic amphiphilic α-helical peptides may be ordered in self-assembled monolayers and supported hybrid bilayers formed on smooth gold surfaces.

Self-assembled monolayers (SAMs) of alkanethiols on gold have been studied extensively in the scientific literature by a number of techniques including surface wetting, atomic force microscopy, spectroscopic ellipsometry, scanning electron microscopy, and X-ray photoelectron spectroscopy.[13,18−29] In recent years, electrochemical techniques have emerged as important tools for characterizing SAMs and supported lipid bilayers on metal surfaces.

Tong and colleagues have performed a body of work in which they used electrochemical methods to study alkanethiol systems

* To whom correspondence should be addressed. Phone: 919-515-7121. Fax: 919-515-3465. E-mail: peter-k@eos.ncsu.edu.

(1) Ding, L.; Li, J. H.; Wang, E. K.; Dong, S. J. *Thin Solid Films* **1997**, *293* (1−2), 153−158.
(2) Gizeli, E.; Liley, M.; Lowe, C. R.; Vogel, H. *Anal. Chem.* **1997**, *69* (23), 4808−4813.
(3) Steinem, C.; Janshoff, A.; Galla, H.-J.; Sieber, M. *Bioelectrochem. Bioenerg.* **1997**, *42* (2), 213−220.
(4) Tien, H. T.; Ottova, A. L. *Colloids Surf A-Physicochem. Eng. Aspects* **1999**, *149* (1−3), 217−233.
(5) Naumann, R.; Baumgart, T.; Graber, P.; Jonczyk, A.; Offenhausser, A.; Knoll, W. *Biosens. Bioelectron.* **2002**, *17* (1−2), 25−34.
(6) Peng, Z. Q.; Tang, J. L.; Han, X. J.; Wang, E. K.; Dong, S. J. *Langmuir* **2002**, *18* (12), 4834−4839.
(7) Wiegand, G.; Arribas-Layton, N.; Hillebrandt, H.; Sackmann, E.; Wagner, P. *J. Phys. Chem. B* **2002**, *106* (16), 4245−4254.
(8) Schmidt, E. K.; Liebermann, T.; Kreiter, M.; Jonczyk, A.; Naumann, R.; Offenhausser, A.; Neumann, E.; Kukol, A.; Maelicke, A.; Knoll, W. *Biosens. Bioelectron.* **1998**, *13* (6), 585−591.
(9) Shen, W. W.; Boxer, S. G.; Knoll, W.; Frank, C. W. *Biomacromolecules* **2001**, *2* (1), 70−79.
(10) Duschl, C.; Liley, M.; Lang, H.; Ghandi, A.; Zakeeruddin, S. M.; Stahlberg, H.; Dubochet, J.; Nemetz, A.; Knoll, W.; Vogel, H. *Mater. Sci. Eng. C* **1996**, *4* (1), 7−18.
(11) Diao, P.; Jiang, D. L.; Cui, X. L.; Gu, D. P.; Tong, R. T.; Zhong, B. *Bioelectrochem. Bioenerg.* **1999**, *48* (2), 469−475.
(12) Knoll, W.; Frank, C. W.; Heibel, C.; Naumann, R.; Offenhausser, A.; Ruhe, J.; Schmidt, E. K.; Shen, W. W.; Sinner, A. *Rev. Mol. Biotechnol.* **2000**, *74* (3), 137−158.
(13) Zhang, L.; Vidu, R.; Waring, A. J.; Lehrer, R. I.; Longo, M. L.; Stroeve, P. *Langmuir* **2002**, *18* (4), 1318−1331.
(14) Krysinski, P.; Moncelli, M. R.; Tadini-Buoninsegni, F. *Electrochim. Acta* **2000**, *45* (12), 1885−1892.
(15) Zebrowska, A.; Krysinski, P.; Lotowski, Z. *Bioelectrochemistry* **2002**, *56* (1−2), 179−184.
(16) Cui, X. L.; Jiang, D. L.; Diao, P.; Li, J. X.; Tong, R. T.; Wang, X. K. *Bioelectrochem. Bioenerg.* **1999**, *48* (1), 243−247.
(17) Boubour, E.; Lennox, R. B. *J. Phys. Chem. B* **2000**, *104* (38), 9004−9010.
(18) Ulman, A. *Chem. Rev.* 1996, *96* (4), 1533−1554.
(19) Ulman, A.; Evans, S. D.; Shnidman, Y.; Sharma, R.; Eilers, J. E. *Adv. Colloid Interface Sci.* **1992**, *39*, p 175−224.
(20) Deng, W. L.; Yang, D. B.; Fang, Y.; Bai, C. L. *Sci. Chin. Ser. B−Chem.* **1996**, *39* (3), 225−234.
(21) Tamada, K.; Hara, M.; Sasabe, H.; Knoll, W. *Langmuir* **1997**, *13* (6), 1558−1566.
(22) Chen, S. F.; Li, L. Y.; Boozer, C. L.; Jiang, S. Y. *Langmuir* **2000**, *16* (24), 9287−9293.
(23) Ishida, T.; Nishida, N.; Tsuneda, S.; Hara, M.; Sasabe, H.; Knoll, W. *Jpn. J. Appl. Phys. Part 2-Lett.* **1996**, *35* (12B), L1710-L1713.
(24) Chen, S. F.; Li, L. Y.; Boozer, C. L.; Jiang, S. Y. *J. Phys. Chem. B* **2001**, *105* (15), 2975−2980.
(25) Yan, C.; Zharnikov, M.; Golzhauser, A.; Grunze, M. *Langmuir* **2000**, *16* (15), 6208−6215.
(26) Rong, H. T.; Frey, S.; Yang, Y. J.; Zharnikov, M.; Buck, M.; Wuhn, M.; Woll, C.; Helmchen, G. *Langmuir* **2001**, *17* (5), 1582−1593.
(27) Colavita, P. E.; Doescher, M. S.; Molliet, A.; Evans, U.; Reddic, J.; Zhou, J.; Chen, D.; Miney, P. G.; Myrick, M. L. *Langmuir* **2002**, *18* (22), 8503−8509.
(28) Wang, Z.; Shi, Y. L.; Li, H. L. *Can. J. Chem.* **2001**, *79* (3), 328−336.
(29) Tsai, M. Y.; Lin, J. C. *J. Colloid Interface Sci.* **2001**, *238* (2), 259−266.

10.1021/la051104w CCC: $33.50
Published on Web 01/20/2006

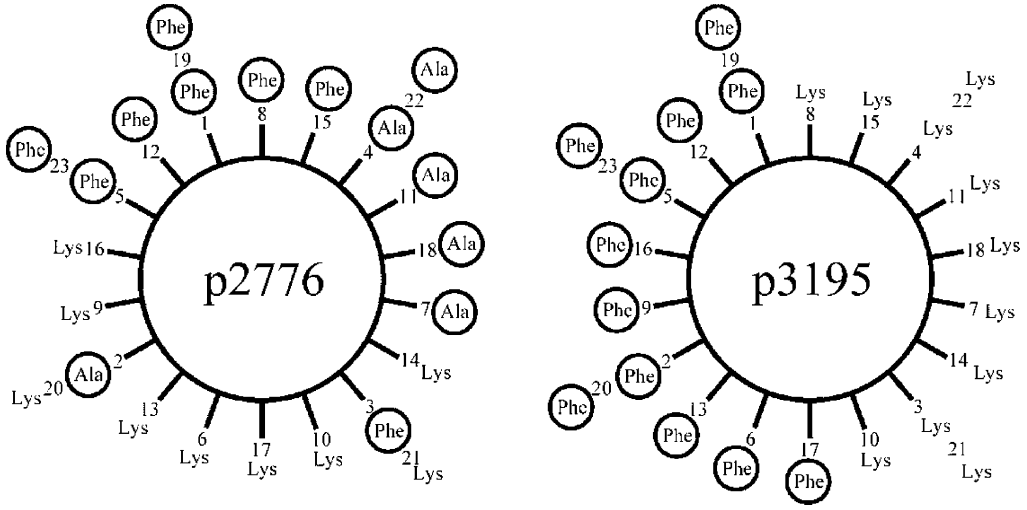

Figure 1. Schiffer−Edmundson wheel diagrams[60] for the two 23-residue synthetic peptides. Hydrophobic side-chains are circumscribed by a circle. The amphiphilicity is apparent from the opposing hydrophobic and hydrophilic faces.

on gold. In a paper by Cui et al.,[30] they used impedance spectroscopy and cyclic voltammetry to study dodecanethiol (DDT) and octadecanethiol (ODT) SAMs under varying concentrations of $Fe(CN)_6^{(3-/4-)}$. Using equivalent circuit modeling, they determined that the resistive element of the SAMs decreased with increasing electrolyte concentration while the capacitive element remained constant. From calculated electron tunneling, they concluded that the apparent effective film thickness was significantly smaller than the alkyl chain lengths, and they suggested that this parameter can serve as a measure of the quality of the SAM. Diao et al.[31] reported that the apparent electron-transfer rate constant for ODT SAMs is several orders of magnitude higher than the theoretical value, suggesting that the discrepancy is due to electron tunneling at "collapsed sites", defects in the SAM resulting at domain boundaries or from inhomogeneities in the underlying gold substrate. At such locales, the thiol molecules do not form a well-ordered lattice, thus permitting the electroactive species to partially penetrate the SAM. The degree of ordering varied among samples, and they attributed constant-phase-element (CPE) behavior to SAM surface roughness. Diao et al.[11] investigated supported hybrid bilayers of ODT and phosphatidylcholine (PC) using CV and EIS. Through equivalent circuit modeling, they determined the bilayer capacitance of this system to be 0.52 $\mu F \cdot cm^{-2}$. They determined that electron transfer through the SAM alone is primarily due to electron tunneling, whereas electron transfer through the hybrid bilayer is due to the diffusion of the electrolyte species through pinhole defects in the PC leaflet. They suggest that the higher occurrence of defects in the bilayer leaflet is attributable to the lipid molecules' inability to form a highly ordered layer over collapsed sites in the underlying SAM. They demonstrate the use of capacitance-plane plots for observing the effects of bilayer addition.

Janek et al. studied SAMs of decanethiol, hydroxydecanethiol, and 4′-hydroxy-4-mercaptobiphenyl using cyclic voltammetry and impedance spectroscopy and analyzed the data using equivalent circuit models.[32] They observed that the electrical behavior of SAMs of decanethiol and hydroxydecanethiol is modeled well using simple equivalent circuit models (e.g., the Randles circuit), whereas the interfacial electrical behavior of the aromatic molecule necessitates a more complex model. They report a double-layer capacitance for decanethiol of $1.49 \pm 0.13\,\mu F \cdot cm^{-2}$.

Protsailo and Fawcett used electrochemical techniques to show that the resistance to charge transfer across alkanethiol SAMs increases with alkyl chain length.[33] They determined that all four thiols investigated (ranging in length from 9 to 18 carbons) form SAMs with a low occurrence of pinhole defects and that conductance through the film is attributable primarily to electron tunneling. In the case of electron tunneling alone, redox current, and thus the standard rate constant k_s, is expected to decay exponentially with increasing film thickness. Indeed, this group observed a linear relationship between the logarithm of the standard rate constant and the alkyl chain length.

Supported hybrid bilayers more closely resemble naturally occurring plasma membranes in that they consist of both an underlying SAM and an overlying phospholipid leaflet. Presumably, such an assembly generates a hydrophilic film surface in which lipid molecules are laterally mobile. These types of films are typically formed by fusing a lipid leaflet onto an existing self-assembled monolayer by one of several approaches including vesicle fusion,[10,34−36] Langmuir−Blodgett deposition,[35,37] or by a painted-lipid/paint-freeze method.[1,35,37−39] These bilayer films are also readily characterized by electrochemical techniques.

In this work, we report on the interactions of several artificially constructed helical peptides with the aforementioned solid-supported films. Many naturally occurring antimicrobial peptides, including melittin and magainins, are known to form membrane-spanning hydrophilic pores under certain conditions.[40−45] In vivo, this creation of ion-conducting channels in the biomembrane

(30) Cui, X. L.; Jiang, D. L.; Diao, P.; Li, J. X.; Tong, R. T.; Wang, X. K. *J. Electroanal. Chem.* **1999**, *470* (1), 9−13.
(31) Diao, P.; Jiang, D. L.; Cui, X. L.; Gu, D. P.; Tong, R. T.; Zhong, B. *J. Electroanal. Chem.* **1999**, *464* (1), 61−67.
(32) Janek, R. P.; Fawcett, W. R.; Ulman, A. *Langmuir* **1998**, *14*, 3011−3018.
(33) Protsailo, L. V.; Fawcett, W. R. *Electrochim. Acta* **2000**, *45* (21), 3497−3505.
(34) Kalb, E.; Frey, S.; Tamm, L. K. *Biochim. Biophys. Acta* **1992**, *1103* (2), 307−316.
(35) Steinem, C.; Janshoff, A.; Ulrich, W. P.; Sieber, M.; Galla, H. J. *Biochim. Biophys. Acta* **1996**, *1279* (2), 169−180.
(36) Lingler, S.; Rubinstein, I.; Knoll, W.; Offenhausser, A. *Langmuir* **1997**, *13* (26), 7085−7091.
(37) Ding, L.; Li, J. H.; Dong, S. J.; Wang, E. K. *J. Electroanal. Chem.* **1996**, *416* (1−2), 105−112.
(38) Jing, W. G.; Wang, E. K. *Anal. Sci.* **1998**, *14* (1), 117−120.
(39) Li, J. H.; Ding, L.; Wang, E. K.; Dong, S. J. *J. Electroanal. Chem.* **1996**, *414* (1), 17−21.
(40) Ladokhin, A. S.; White, S. H. *J. Mol. Biol.* **1999**, *285* (4), 1363−1369.
(41) Oren, Z.; Ramesh, J.; Avrahami, D.; Suryaprakash, N.; Shai, Y.; Jelinek, R. *Eur. J. Biochem.* **2002**, *269* (16), 3869−3880.
(42) Chen, F. Y.; Lee, M. T.; Huang, H. W. *Biophys. J.* **2003**, *84* (6), 3751−3758.
(43) Bechinger, B. *Biochim. Biophys. Acta-Biomembr.* **1999**, *1462* (1−2), 157−183.

leads to death of the target cell by disrupting both the structural integrity and the ion-mediating properties of the victim cell's plasma membrane. These pore-forming peptides have been studied for several decades and continue to be an active topic of scientific research. The pore-forming behavior of these peptides is attributed to their amphiphilic α-helical design, in which the amino acid functional groups of one face of the α-helix are largely hydrophobic while those of the opposing face are largely hydrophilic (cf. Figure 1). Melittin, for example, is believed to form molecular aggregates on the surfaces of cellular membranes which then insert themselves into the lipid bilayer to form pore structures.[46,47] The peptides aggregate such that the hydrophobic faces of the individual peptides orient outward while the hydrophilic faces orient inward, toward the aqueous pore.

Issues such as understanding the mechanisms by which these peptides insert themselves into cellular membranes and form aggregates as well as how the structural characteristics of these aggregates (e.g., number of monomers per aggregate, pore diameter, ion selectivity, etc.) may be directly controlled though solvent conditions and primary sequence design are of significant scientific and technological interest. In the present work, we have fabricated hybrid lipid bilayers on gold by depositing a lipid bilayer leaflet on a preexisting SAM using the paint-freeze method of bilayer formation.[1,35,37,38] Monolayers were formed using straight-chain alkanethiols and 1,2-dipalmitoyl-*sn*-glycero-3-phosphothioethanol (DPPTE). Synthetic helical peptides were introduced to the bilayer at various stages of the membrane formation and at varying concentrations and peptide-to-lipid molar ratios. The physicochemical characteristics of these surfaces were assessed by utilizing a number of experimental tools, including electrochemical impedance spectroscopy (EIS) and near-edge X-ray absorption fine structure (NEXAFS) spectroscopy.

Materials and Methods

Materials. Absolute ethanol was purchased from Aldrich; all other solvents were purchased from Fisher Scientific and used as received. Gold substrates were prepared by C. Richard Guarnieri (NC State University) and by Soojin Oh (UNC Chapel Hill). Gold films with thicknesses of 100−150 nm were vapor-deposited on silicon wafers covered previously with 20-nm chromium adhesion layers. The root-mean-square surface roughness of these gold wafers, as determined by atomic force microscopy prior to experimentation, was ≈9 Å. Dodecanethiol (DDT) and octadecanethiol (ODT) were purchased from Sigma-Aldrich and were used as received. 1,2-Dipalmitoyl-*sn*-glycero-3-phosphothioethanol (DPPTE) was purchased in chloroform solution from Avanti Polar Lipids, Inc. 1,2-Dimyristoyl-*sn*-glycero-3-phosphocholine (DMPC); 1-palmitoyl-2-oleoyl-*sn*-glycero-3-phosphocholine (POPC); and 1-palmitoyl-2-oleoyl-*sn*-glycero-3-[phospho-*rac*-(1-glycerol)] (Sodium Salt) (POPG) were purchased from Avanti Polar Lipids in dry powdered form and were used without further purification. Potassium chloride was purchased from Fisher Scientific. Aqueous solutions of potassium ferrocyanide and potassium ferricyanide were purchased from LabChem, Inc.

Melittin was purchased from Sigma-Aldrich and used without further purification. Synthetic peptides were manufactured by Biopeptide Co., LLC (San Diego, CA) and delivered in lyophilized form. Two synthetic 23-residue peptides were synthesized using three amino acids: alanine, phenylalanine, and lysine (cf. Table 1 and Figure 1). Alanine and phenylalanine are both uncharged and form the hydrophobic face of the α-helix, while lysine contains a charged quaternary ammonium group and forms the hydrophilic face of the peptide. To facilitate peptide adhesion to the gold surface, these two sequences were reproduced with the addition of a cysteamine group at the C-terminus. The presence of the mercapto functionality on the peptide facilitated the bonding of the peptide to the gold substrate. Herein, the original synthetic peptides are referred to by their molecular weights, p2776 and p3195, and the cysteamine-terminating peptides are referred to as p2776-SH and p3195-SH, respectively.

Table 1. Four Synthetic Peptides Were Manufactured Based on Two Sequences[a]

	sequence[b]	residues	MW
1	FAFAFKAFKKAFKKFKKAFKKAF−OH	23	2776
2	FFKKFFKKFKKFFKKFFKFFKKF−OH	23	3195
3	FAFAFKAFKKAFKKFKKAFKKAF−NH−$(CH_2)_2$−SH	23	2835
4	FFKKFFKKFKKFFKKFFKFFKKF−NH−$(CH_2)_2$−SH	23	3254

[a] Versions were made with and without a terminal sulfur-containing cysteamine residue. [b] Three amino acids were used: A, alanine; F, phenylalanine; and K, lysine.

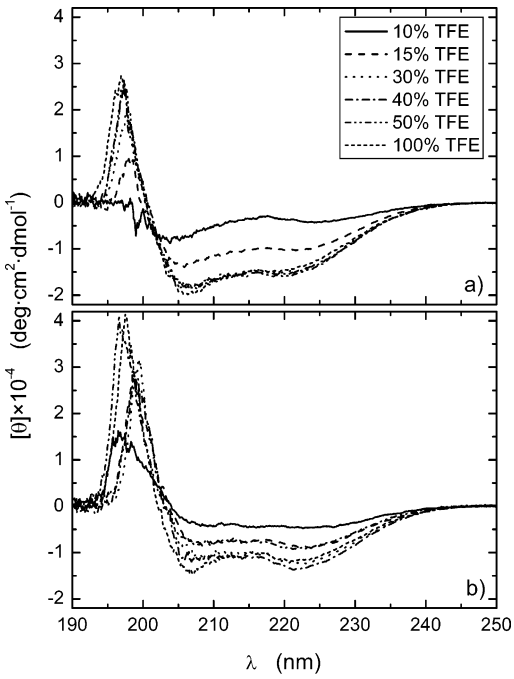

Figure 2. Circular dichroism of the two 23-residue synthetic peptides, (a) p2776 and (b) p3195, in several concentrations of TFE in PBS buffer confirms the peptides' helicity. A concentration of 0.5 mg/mL was tested in a 1-mm path length cell.

Circular Dichroism. The helicity of our synthetic peptides was confirmed by circular dichroism using a Jasco J600 spectropolarimeter. Data were collected at room temperature using a 1-mm path length cell. The circular dichroism of the two peptides p2776 and p3195 was confirmed and quantified in mixtures of trifluoroethanol (TFE) and pH 7.4 phosphate buffered saline (cf. Figure 2). Melittin was also characterized under the same conditions as a point of reference for our novel peptides. Additionally, the helicity of the synthetic peptides in vesicles was characterized by performing circular dichroism experiments on dispersions of vesicles. The degree of helicity was quantified using the empirical equation adapted from the work of Chen et al.[48] and used throughout the literature:[49,50]

(44) Vogt, T. C. B.; Bechinger, B. *J. Biol. Chem.* **1999**, *274* (41), 29115−29121.
(45) Bechinger, B. *J. Membr. Biol.* **1997**, *156* (3), 197−211.
(46) Matsuzaki, K.; Yoneyama, S.; Miyajima, K. *Biophys. J.* **1997**, *73* (2), 831−838.
(47) Yang, L.; Harroun, T. A.; Weiss, T. M.; Ding, L.; Huang, H. W. *Biophys. J.* **2001**, *81* (3), 1475−1485.
(48) Chen, Y. H.; Yang, J. T.; Chau, K. H. *Biochemistry* **1974**, *13* (16), 3350−3359.
(49) Mozsolits, H.; Wirth, H. J.; Werkmeister, J.; Aguilar, M. I. *Biochim. Biophys. Acta-Biomembr.* **2001**, *1512* (1), 64−76.
(50) Vila, R.; Ponte, I.; Collado, M.; Arrondo, J. L. R.; Jimenez, M. A.; Rico, M.; Suau, P. *J. Biol. Chem.* **2001**, *276* (49), 46429−46435.

$$f_H = \frac{[\theta]_{222}}{-39\,500\left(1 - \frac{2.57}{n}\right)}$$

where $[\theta]_{222}$ is the mean residue ellipticity at 222 nm and n is the number of amino acid residues involved in the α-helix.

Electrochemical Impedance Spectroscopy (EIS). Electrochemical impedance spectroscopy was carried out on a Zahner IM6e Electrochemical Workstation (Zahner, Germany). A conventional three-electrode electrochemical cell was designed with a large area platinum counter electrode and a saturated Ag/AgCl reference electrode. The sample served as the working electrode and had an exposed surface area of 0.2 cm^2. The aqueous electrolyte solution used for EIS experiments was 2 mM in each of potassium ferricyanide ($K_3Fe[CN]_6$) and potassium ferrocyanide ($K_4Fe[CN]_6$) and 0.1 M in KCl. The electrolyte was deoxygenated by sparging with nitrogen gas for 30 min. All experiments were conducted at ambient temperature. EIS data were collected in potentiostat mode with a voltage amplitude of 10 mV at open circuit potential over the frequency range of 100 mHz to 100 kHz. The data were then analyzed by fitting to equivalent circuit models using a complex least-squares analysis within the ZSimpWin software package (EChem Software).

Near-Edge X-ray Absorption Fine Structure Spectroscopy (NEXAFS). NEXAFS spectroscopy experiments were conducted on the NIST/Dow X-ray facility (beamline U7A) of the National Synchrotron Light Source at Brookhaven National Laboratory (Upton, NY). NEXAFS uses low-energy X-rays to detect bond population and the orientation of molecules on surfaces. The intensity of the NEXAFS signal is a function of (1) density of molecules on the surface and (2) the angle between the electric field polarization vector of the incident light and the antibonding orbitals of the surface molecules being studied. In our work, NEXAFS is used to determine the molecular orientation of SAM-forming molecules and phospholipid moieties as well as to verify the presence of the peptides in the supported film on the surface.

Contact Angle. Contact angle provides a convenient means of characterizing the surface energies and complex structures of our samples. For liquid droplets on a homogeneous surface, a characteristic angle is formed at the interface of the solid, liquid, and vapor phases. In the case of deionized water, hydrophilic surfaces will result in small contact angles (e.g., 10−50°), whereas hydrophobic surfaces will result in large contact angles (e.g., 100−110°). Furthermore, the hysteresis between the advancing and receding contact angles provides information about heterogeneity of the surface; a hysteresis smaller than ≈10° is generally considered to signify a relatively uniform surface. Whereas gold is highly hydrophilic, self-assembled alkanethiol monolayers create highly hydrophobic surfaces. Therefore, we can use contact angle to verify the presence and quality of oriented self-assembled monolayers on gold. Contact angle experiments were conducted on a Ramé-Hart contact angle goniometer (model 100−00). For advancing contact angles, 8 mL of deionized water were delivered onto the surface. At least 10 measurements were taken and averaged while maintaining contact between the syringe needle and the water droplet. For receding contact angles, 4 mL of deionized water were drawn back into the syringe. Again, at least 10 measurements were taken and averaged to yield a single value.

Sample Preparation. Gold substrates were cut to sizes of approximately 1 cm^2 for all experiments. Before film deposition, the cut substrates were cleaned by ultraviolet/ozone (UV/O) treatment for 15 min, sonicated in absolute ethanol (30 min), and sonicated in fresh piranha solution (three parts H_2SO_4 to one part technical grade H_2O_2; 5 min.). SAMs of DDT, ODT, and DPPTE were formed by immersing the cleaned gold substrates in thiol solutions for an extended period of time. For all data presented herein, depositions were performed in excess of 16 h. ODT and DDT depositions were carried out in 2 mM ethanolic solutions. Also, 2 mM solutions of DPPTE were made in each of four different solvents: chloroform, methylene chloride, tetrahydrofuran, and a 1:1 mixture of toluene and ethanol.

Table 2. Percent Peptide Helicity Determined Empirically for Several Peptides Using Circular Dichroism

system	FW/Da	n	$[\theta]_{222} \times 10^{-4}$/ deg·$cm^2$·$dmol^{-1}$	helicity f_H
melittin in 40% TFE in PBS	2846.46	26	−1.77	49.7%
p2776 in 40% TFE in PBS	2776	23	−1.48	42.1%
p3195 in 40% TFE in PBS	3195	23	−1.35	38.4%
POPC/POPG + p2776 20:1	2776	23	−2.92	83.4%
POPC/POPG + p2776 50:1	2776	23	−3.09	87.9%
POPC/POPG + p2776 100:1	2776	23	−2.97	84.6%
POPC/POPG + p3195 20:1	3195	23	−1.52	43.2%
POPC/POPG + p3195 50:1	3195	23	−1.44	41.2%
POPC/POPG + p3195 100:1	3195	23	−1.55	44.3%

Supported lipid bilayers were formed by adding a glycerophospholipid leaflet onto an existing SAM. This was accomplished by one of two methods: (1) the painted-lipid method originally proposed by Florin and Gaub[37,51] and (2) the paint-freeze method described by White.[37,52] In the painted-lipid method of bilayer formation, a small amount of lipid solution was applied on a substrate with a preexisting well-formed monolayer. The painting-solution consisted of a 20 mg/mL solution of glycerophospholipid in a 3:1 mixture of decane and 2-butanol. After "painting", the sample was submersed in an aqueous solution of 0.1 M KCl for a period of 2 h. During this incubation time, the lipid molecules formed a bilayer because of the hydrophobic and hydrophilic interactions with the thiolated monolayer and the aqueous solution. Co-deposition solutions of DMPC and synthetic peptide were similarly prepared that were 20 mg/mL in DMPC and 0.2 mg/mL in peptide. The paint-freeze method for bilayer formation is a modification of the painted-lipid method.[37,52] After the application of the lipid painting-solution, the solvent is frozen out by placing the sample in a −20 °C environment for at least 20 min. The sample is then submersed in KCl solution for an extended period of time, just as in the painted-lipid procedure.

Results and Discussion

Circular Dichroism. Circular dichroism was used to demonstrate that our synthetic peptides definitely assume helical conformation. The peptides were studied both in solution with trifluoroethanol as well as in hydrated lipid vesicles. In Figure 2, we plot circular dichroism spectra of the two 23-residue synthetic peptides, (a) p2776 and (b) p3195, in several concentrations of TFE in PBS buffer. The results are summarized in Table 2 for peptide concentrations of 0.5 mg/mL in 40% TFE. These data confirm that the synthetic peptides p2776 and p3195 form helical secondary structures.

Circular dichroism data were also collected for peptide-incorporated POPC/POPG lipid vesicles to demonstrate that helical conformation is assumed as the peptides incorporate into a lipid bilayer structure (cf. Figure 3). Both peptides p2776 and p3195 were investigated in vesicles formed by extrusion under varying peptide-to-lipid molar ratios (1:20, 1:50, and 1:100) with a constant POPC:POPG molar ratio of 3:1 maintained throughout. Peptide concentration was 0.1 mg/mL for all experiments. These data demonstrate that these synthetic peptides do form helical secondary structures when incorporated into a lipid bilayer leaflet. Furthermore, the helicities obtained in the lipid vesicles is substantially greater than those obtained for the peptides in buffer/TFE alone (cf. Table 2).

Because our synthetic peptides are shown to be able to form helical secondary structures under the two sets of conditions given above, we assume that they are also capable of assuming this helical conformation when inserted in the solid-supported films we describe in this paper.

(51) Florin, E. L.; Gaub, H. E. *Biophys. J.* **1993**, *64* (2), 375−383.
(52) White, S. H. *Biochim. Biophys. Acta* **1974**, *356* (1), 8−16.

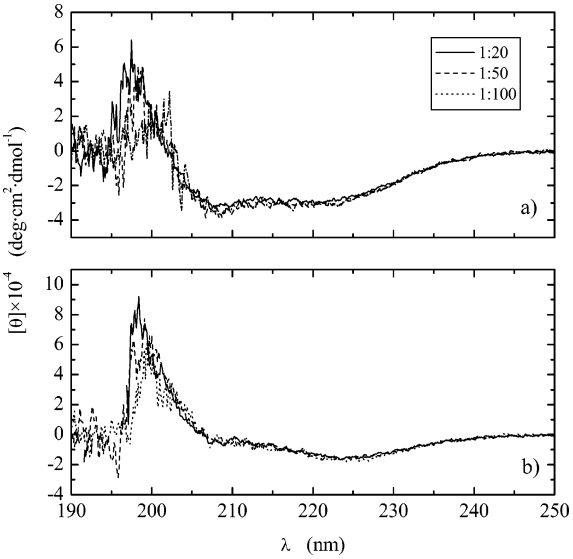

Figure 3. Circular dichroism spectra for POPC/POPG vesicles with inserted peptide 2776 (a) and 3195 (b).

Table 3. Advancing and Receding Contact Angles for DDT, ODT, and DPPTE Monolayers on Gold

	thiol	solvent	contact angle (deg) advancing	receding	hysteresis
1	DDT	EtOH	107°	89°	18°
2	DDT	EtOH	101°	84°	17°
3	DDT	EtOH	105°	87°	18°
4	ODT	EtOH	110°	97°	13°
5	ODT	EtOH	110°	100°	10°
6	ODT	EtOH	109°	98°	11°
7	ODT	EtOH	111°	100°	11°
8	ODT	EtOH	113°	99°	14°
9	DPPTE	1:1 toluene:EtOH	110°	98°	12°
10	DPPTE	1:1 toluene:EtOH	106°	101°	5°
11	DPPTE	CH_2Cl_2	105°	93°	12°

Contact Angle. Advancing contact angles for both the alkanethiol and DPPTE SAMs were quite high (cf. Table 3), indicating the presence of well-ordered SAMs. Advancing contact angles for the DDT and ODT monolayers were similar to those reported for alkanethiols in the literature.[20,53−55] Additionally, the advancing contact angles for ODT were higher than those for DDT. This observed increase in contact angle with alkyl chain length is consistent with the literature reports[20,55] and may be attributable to increased packing density resulting from chain−chain interactions. The absolute values of our contact angles are somewhat lower than those reported in the literature,[20,53−55] however, which may indicate a higher degree of disorder due to gold surface roughness. The contact angles for DPPTE SAMs were slightly lower than those obtained for ODT but were higher than those obtained for DDT, suggesting that ODT either packs more densely than DPPTE or contains a smaller number of structural defects. This improved packing of ODT is attributed to the highly regular linear chain structure of ODT as compared to DPPTE. In the case of DDT, we suggest that the shorter molecular length and higher rigidity of the molecule may account for both its lower advancing contact angles and its higher hysteresis between advancing and receding contact angles.

Electrochemical Impedance Spectroscopy. Several mechanisms may contribute to the total apparent electrical conductivity across our SAMs and supported bilayers including ionic penetration of the film and diffusion of the redox couple to and from the gold surface. Ionic species may approach the electrode surface at pinhole defects in the film, at collapsed sites in the bilayer leaflet, and, in the case of peptide-incorporated films, at distortions or openings promoted by the peptide molecules' attachment to or insertion into the film. It is also possible for the presence of charged peptides in the hybrid bilayer to alter the apparent electrical permeability of the bilayer films through electrostatic attraction or repulsion of ionic species. For our analysis, we have elected to simplify the modeling by treating our systems as having a single resistive element in parallel with a single capacitive element.

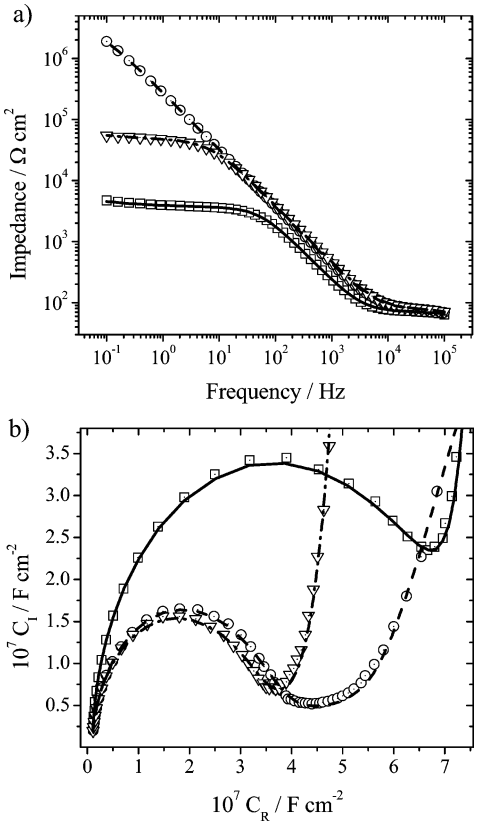

Figure 4. Bode impedance plot (a) and capacitance-plane plot (b) for a DPPTE/DMPC bilayer system with peptide p3195-SH. A DPPTE monolayer (□) was first formed. A DMPC bilayer leaflet was subsequently applied (○). Finally, the DMPC leaflet was removed and the monolayer was painted with a solution containing DMPC and peptide p3195-SH (▽). Also shown is the (C(R(Q(RW)))) equivalent circuit model for each curve.

Data were collected for bilayer systems for each stage of their fabrication. Data were first collected for the monolayer alone, consisting of either pure alkanethiol (DDT or ODT) or pure DPPTE. The sample was then rinsed thoroughly in its respective deposition solvent, and a DMPC bilayer was applied using the paint-freeze method of bilayer formation. After electrochemical data were collected for the bilayer system, the sample was rinsed with methylene chloride to completely remove the bilayer leaflet. Finally, a bilayer including peptide was formed using the paint-freeze method with a solution containing both DMPC and peptide. It should be noted that we observed a great degree of variability in the electrical behavior of otherwise identical samples prepared on different substrates. We attribute this to variations in surface roughness and defects among several substrates. The following electrochemical data are from representative samples.

(53) Bain, C. D.; Troughton, E. B.; Tao, Y. T.; Evall, J.; Whitesides, G. M.; Nuzzo, R. G. *J. Am. Chem. Soc.* **1989**, *111* (1), 321−335.
(54) Ron, H.; Matlis, S.; Rubinstein, I. *Langmuir* **1998**, *14* (5), 1116−1121.
(55) Laibinis, P. E.; Whitesides, G. M. *J. Am. Chem. Soc.* **1992**, *114* (6), 1990−1995.

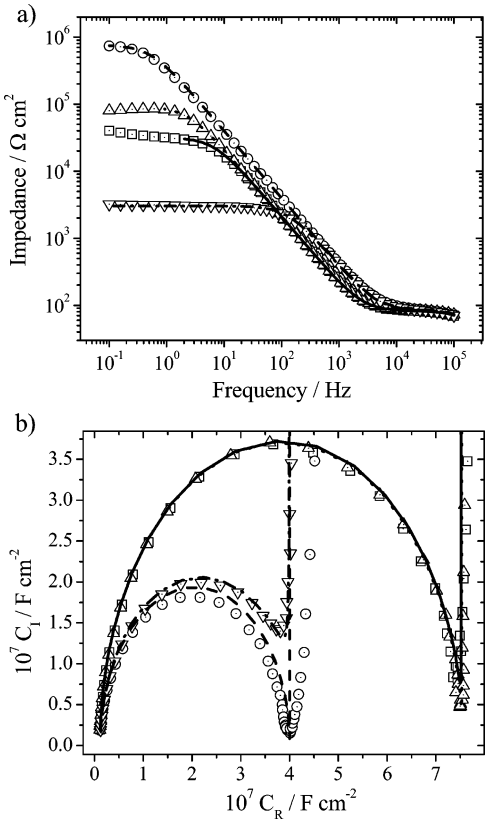

Figure 5. Bode impedance plot (a) and capacitance-plane plot (b) for a DDT/DMPC bilayer system with peptide p3195-SH. First a DDT SAM was formed (□), to which a DMPC bilayer leaflet was subsequently added (○). The DMPC was then rinsed off (△) and the monolayer was painted with a solution containing both DMPC and peptide p3195-SH (▽). Also shown is the (C(R(CR))) equivalent circuit model for each curve.

In Figures 4 and 5, we plot the EIS results for DPPTE/DMPC and DDT/DMPC bilayer systems, respectively. The magnitude of the impedance curve for the DPPTE monolayer is substantially smaller than that for the DDT monolayer. Furthermore, the frequency range for which the DPPTE monolayer displays primarily capacitive behavior is significantly narrower than that for the DDT monolayer. We suggest that these observations indicate that the DDT SAM has a lower incidence of pinhole or collapsed site defects than the DPPTE SAM. Although the DPPTE SAM appears to have a higher packing density and degree of ordering within ordered domains, as evidenced by contact angle, its more irregular structure may lead to the formation of a greater number of defects at domain boundaries and substrate inhomogeneities.

Upon introduction of a DMPC bilayer leaflet to the monolayer, the impedance increases over the entire observed frequency range. Additionally, the system displays capacitive behavior over a wider range of frequencies. Although the system becomes more resistive to electron flow, the magnitude of the capacitance of the film decreases, as is observed by the decrease in the diameter of the arc formed in the capacitance-plane plot. The diameter of the arc in the capacitance-plane plot is inversely related to the thickness of the film (cf. Figures 4 and 5).[35−37,56−58] Additionally, the curvature of the data in the capacitance-plane plots differs greatly between the DDT system and the DPPTE system. The substitution of the constant phase element (CPE) for an ideal capacitor in the modeling of the DPPTE system allows us to capture this curvature, which is a result of higher surface roughness.[31] We posit that this greater surface roughness is a result of a higher incidence of pinhole defects and collapsed sites in the DPPTE SAM as opposed to the DDT SAM.

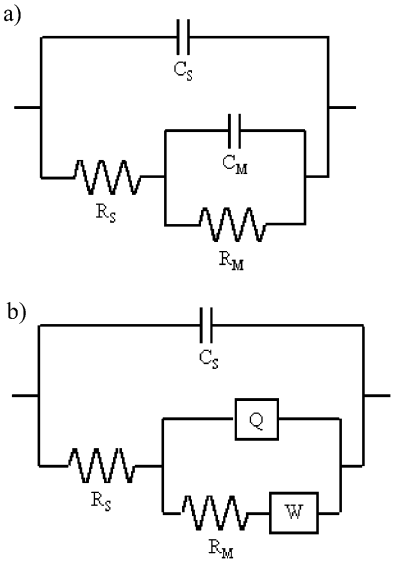

Figure 6. Two of several equivalent circuit models used for the EIS data fitting are presented. The DDT system was modeled with the first circuit (a), which uses a capacitor and resistor to model both the electrolyte (C_S and R_S) as well as the organic film (C_M and R_M). For the DPPTE system, the second circuit (b) modeled the data better. This circuit uses a constant phase element (Q) instead of a capacitor to model the film "capacitance" and introduces a Warburg element to capture diffusion limitations in the low-frequency regime.

Table 4. EIS Modeling Parameters for the Several Stages of Fabrication for the DPPTE/DMPC/Peptide System Presented in Figure 4[a]

3195SH-incorporated DPPTE/DMPC bilayer			
	DPPTE SAM	+ DMPC	+ DMPC and peptide
C/nF·cm^{-2}	10.	10.	9.4
R_S/Ω·cm^2	72	80.	80.
Q/μS·s$^{0.5}$·cm^{-2}	0.99	0.63	0.61
n	0.96	0.94	0.93
R_M/Ω·cm^2	3.6×10^3	3.1×10^6	4.7×10^4
W/S·s$^{0.5}$·cm^{-2}	1.1×10^{-3}	9.0×10^{-7}	1.1×10^{-4}
	$\chi 2 = 3.7 \times 10^{-4}$	$\chi 2 = 1.5 \times 10^{-4}$	$\chi 2 = 2.3 \times 10^{-4}$

[a] This system was modeling as (C(R(Q(RW)))).

Figure 5 also shows the electrochemical impedance data gathered after the DDT/DMPC bilayer sample was rinsed thoroughly with methylene chloride to remove the bilayer leaflet. The Bode impedance curve drops to values near those of the DDT monolayer alone for most of the recorded frequency range, and the diameter of the arc in the capacitance-plane plot returns to that for the monolayer data.

Upon the addition of a solution containing both DMPC and peptide p3195-SH, the impedance drops and the diameter of the arc of the capacitance-plane plot returns approximately to the value detected for the bilayer sample, indicating that the film is still intact (cf. Figures 4 and 5).

The EIS data were fit to equivalent circuit models using the ZSimpWin 2.00 (EChem Software) software package. Equivalent circuit modeling permits the quantification of the electrical behaviors of individual system components. In Figure 6, we present two such models that fit best our experimental data. The circuit shown in Figure 6a builds on the simple Randles circuit

(56) Porter, M. D.; Bright, T. B.; Allara, D. L.; Chidsey, C. E. D. *J. Am. Chem. Soc.* **1987**, *109* (12), 3559−3568.
(57) Xu, J.; Li, H.-l. *J. Colloid Interface Sci.* **1995**, *176* (1), 138−149.
(58) Plant, A. L. *Langmuir* **1993**, *9* (11), 2764−2767.

Table 5. EIS Modeling Parameters for the Several Stages of Fabrication for the DDT/DMPC/Peptide System Presented in Figure 5[a]

	3195SH-incorporated DDT/DMPC bilayer			
	DDT SAM	+ DMPC	rinsed	+DMPC & peptide
C_S/nF·cm^{-2}	11	11	11	12
R_S/Ω·cm^2	83	90.	86	87
C_M/μF·cm^{-2}	0.75	0.39	0.74	0.41
R_M/kΩ·cm^2	32	760	91	2.9
	$\chi 2 = 6.8 \times 10^{-4}$	$\chi 2 = 2.4 \times 10^{-3}$	$\chi 2 = 1.1 \times 10^{-4}$	$\chi 2 = 8.9 \times 10^{-4}$

[a] This system was modeled as (C(R(CR))).

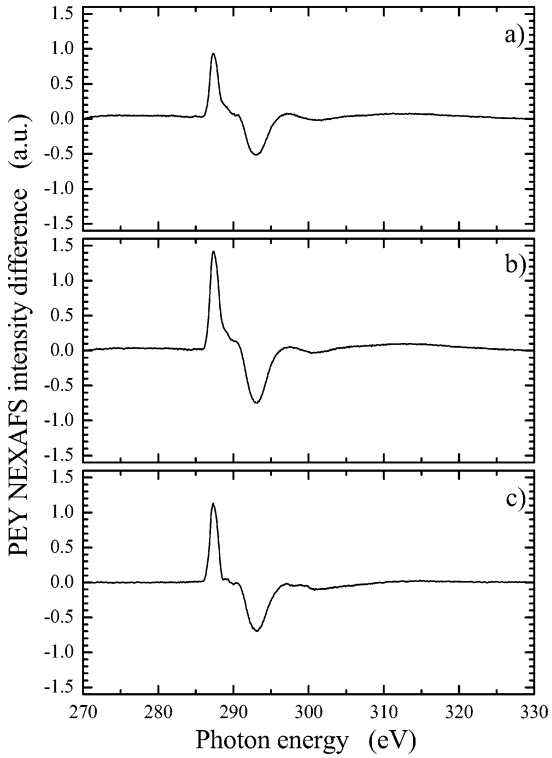

Figure 7. Difference NEXAFS spectra for (a) ODT SAM, (b) DPPTE SAM, and (c) DMPC multilayer formed on DPPTE. The difference spectra were obtained by subtracting the NEXAFS spectra collected at normal incident ($\theta = 90°$) and glancing incidence ($\theta = 20°$ for a and b and $\theta = 35°$ for c) geometries.

(not discussed here) by adding a second capacitor (C_S) to model the electrolyte capacitance. The addition of this circuit element improves modeling in the high-frequency regime and permits us to confirm that the electrical properties of the electrolyte remain constant throughout consecutive experiments. This circuit, called (C(R(CR))) herein, was used to model the DDT system presented in Figure 5. The circuit presented in Figure 6b, herein referred to as (C(R(Q(RW)))), is increased in complexity. The substitution of a constant phase element (Q) for the film capacitance allows us to better model the capacitive behavior of surfaces with greater surface inhomogeneity. Additionally, the use of a Warburg element (W) allows us to account for diffusion effects in the low-frequency regime. This circuit was used to model the DPPTE system presented in Figure 4.

Table 4 provides the equivalent circuit modeling parameters for the three sequential steps of a peptide-inserted hybrid bilayer fabrication shown in Figure 4: DPPTE SAM formation, bilayer deposition, and peptide-incorporated bilayer deposition. For each step of the sample formation, equivalent circuit modeling confirms that the capacitance and resistance of the electrolyte solution remain constant. Because the values of the constant phase element exponent, *n*, are always close to unity, we assume that the magnitude of the constant phase element offers a good estimate

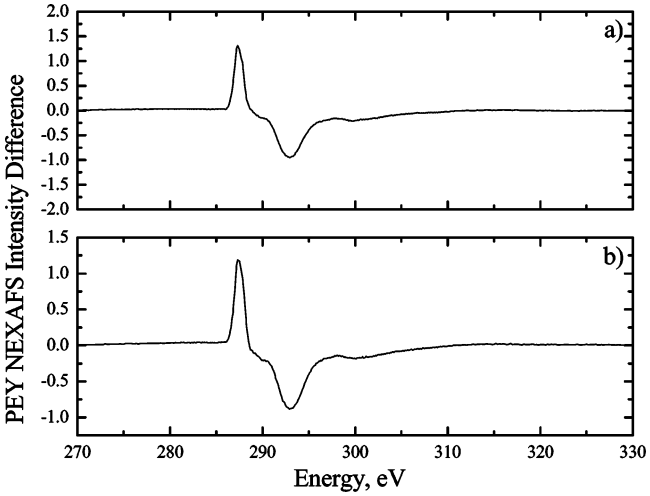

Figure 8. NEXAFS difference spectra (90°−20°) for DMPC multilayers with incorporated peptide p3195-SH on ODT (a) and DPPTE (b) monolayers. Peptide does not disrupt the orientation of the surrounding aliphatic material.

of the capacitance of the membrane.[30,33] Upon painting the structure with the lipid, the magnitude of the film capacitance drops. This capacitance then remains approximately constant upon the formation of a bilayer with peptide. The resistance of the membrane increases greatly upon painting and drops significantly for the bilayer upon the peptide insertion. The capacitances obtained for this system are on the same order of magnitude as capacitances obtained for similar systems reported in the literature.[11,30,33,35,37,58]

Table 5 provides the modeling parameters for the peptide-incorporated system on DDT presented in Figure 5. Just as in the preceding case, the electrolyte components of the model (C_S and R_S) remain constant throughout. Upon addition of a DMPC leaflet to the DDT monolayer, the membrane capacitance (C_M) drops substantially; the resistive component (R_M) increases by over an order of magnitude. Upon stripping the DMPC leaflet, C_M and R_M approach their original values. When the DDT is then painted with the DMPC+peptide solution, C_M returns to the bilayer value and R_M drops substantially. These results are consistent with the expected effects of peptide incorporation with the supported film. The film capacitance is related to the dielectric constant of the organic material and to the thickness of the organic film by the equation[35,58]

$$C_m = \frac{\epsilon_0 \kappa}{d}$$

where C_m is the specific capacitance of the film, ϵ_0 is the permittivity of vacuum, κ is the dielectric constant of the organic material, and d is the film thickness. The dielectric constant for alkyl SAMs is not precisely known as it can vary greatly upon specific conditions and is usually assumed to range from 2.0 to

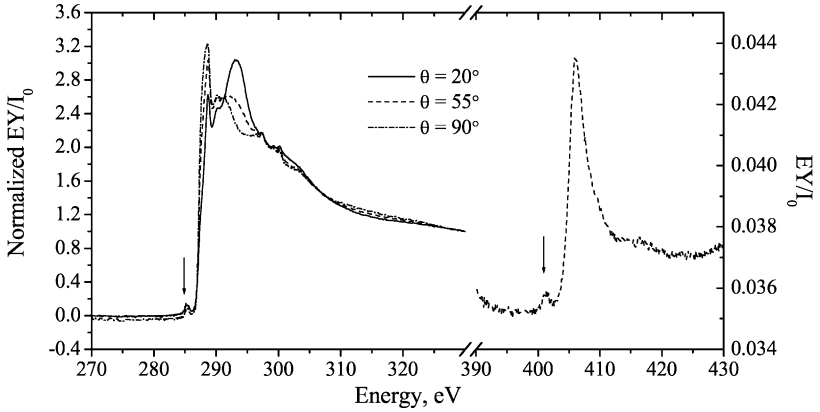

Figure 9. Aromatic ring in the phenylalanine residues yields a strong π^* resonance peak in the carbon K-edge spectrum at ca. 285 eV when larger amounts of peptide are adsorbed to the surface (left). Additionally, the peptide bond yields a characteristic peak in the nitrogen K-edge spectrum at ca. 403 eV (right).

2.5.[33,35−37,51,56,57,59] Because the capacitance of the peptide-incorporated bilayer film returns to the value of the alkanethiol/DMPC bilayer, we deduce that the peptide is incorporating into the film and neither simply removing segments of the DMPC leaflet nor adding additional multilayers. We do, however, expect the peptide to essentially introduce defects into the organic film, and this is reflected in the drop in the value of the resistive element.

It is interesting to note that the specific capacitances of the DPPTE films are greater than those obtained for the DDT films. If the respective systems possessed identical dielectric constants and molecular tilts, one would expect the DPPTE, the longer molecule, to form films with lower capacitances. However, this is not observed. Additionally, the capacitances obtained, although on the same order of magnitude as those reported in the literature, are somewhat smaller than the values reported elsewhere.[11,30,32,33,35,58] These observations may indicate that DPPTE and DDT have markedly different packing densities and thus dielectric constants for their alkyl chains. Alternatively, these data may suggest that DPPTE and DDT have different molecular tilts on our gold substrates and thus their relative SAM thicknesses are not directly related to chain length alone. Regardless of absolute equivalent circuit modeling values, we may still observe the effects of peptide incorporation upon subsequent steps of film assembly in the data presented herein.

Near-Edge X-ray Absorption Fine Structure Spectroscopy. NEXAFS spectroscopy was performed on thiol monolayers, overlying DMPC multilayers, and multilayers with incorporated peptide p3195-SH. Because NEXAFS is performed under vacuum and hence it is not possible to maintain an intact hybrid bilayer out of aqueous solution, lipid multilayers were studied by NEXAFS in lieu of hybrid bilayers. Here we assume that the nanostructure of peptide-incorporated multilayers should resemble that of peptide-incorporated hybrid bilayers. Carbon K-edge data were collected over the photon energy range 270−330 eV. The electron yield spectra were normalized by shifting the preedges (at 270 eV) to zero and subsequently scaling the postedges (at 330 eV) to unity. The converse angular dependences of the C−H and C−C 1s $\rightarrow \sigma^*$ peaks at ca. 288 and 293 eV, respectively, demonstrate that the monolayers are ordered.

Figure 7, panels a and b, presents the carbon K-edge difference spectra (90°−20°) for an ODT and a DPPTE SAM, respectively, and Figure 7c presents the carbon K-edge difference spectrum (90°−35°) for a DMPC multilayer formed on DPPTE. The DMPC multilayers exhibit similar orientation as that shown in the cases of ODT and DPPTE SAMs. Orientation of DMPC is confirmed from the alternate angular dependences of the C−H and C−C 1s $\rightarrow \sigma^*$ peaks.

Figure 8 presents the carbon K-edge difference spectra for DMPC multilayers with incorporated peptide p3195-SH on an ODT (a) and a DPPTE (b) monolayer. The orientation of the carbon chains is still observed from the C−H and C−C peaks. At higher peptide-to-lipid ratios, the presence of peptide can be observed in both the carbon and nitrogen K-edge spectra. Figure 9 presents data collected for DMPC/p3195-SH multilayers formed on a DDT monolayer. The painting solution contained 0.2 mg/mL p3195-SH and 0.833 mg/mL DMPC (a 5:100 peptide: lipid molar ratio) in methanol/chloroform/TFE (3/1/1 v/v). The highly aromatic phenylalanine residues contained in the synthetic peptides have been observed to significantly enhance the C−C 1s $\rightarrow \pi^*$ peak at ca. 285 eV. Additionally, the presence of the peptide bond yields a peak at ca. 403 eV in the nitrogen K-edge regime (cf. Figure 9). The peak at ca.403 eV is entirely absent in control samples containing only thiol molecules, DMPC, or amino acid monomers.

Our synthetic peptides are positively charged since lysine residues carry a positive charge at near-neutral pH. Because electrostatic repulsion between peptides may hinder the formation of peptide aggregates, NEXAFS experiments were conducted in which the effects of solvent electrolyte concentration and solvent water content on peptide co-deposition ability were studied for systems of simultaneously adsorbed DDT and peptide p2776-SH. At a high peptide-to-DDT ratio (20:100), both increased solvent KCl concentration and increased solvent water content resulted in improved peptide adhesion (as determined from the π^* resonance peaks). This solvent phenomenon was not observed, however, at lower peptide-to-DDT ratios.

Conclusion

For the solid-supported bilayer films studied, EIS data have confirmed that a significant change in the electrical properties of the films takes place upon the introduction of synthetic peptide. The electrical resistive element of the surface film decreases, whereas the capacitive element remains comparable to that for a DMPC/thiol hybrid bilayer. These results suggest that peptides insert into well-ordered bilayers and enable electron flow in the immediate vicinity of the peptide molecules. Although these data are compelling, the exact mechanisms of the peptide interactions with the film are not clear and require further study.

(59) Montal, M.; Mueller, P. *Proc. Natl. Acad. Sci. U.S.A.* **1972**, *69* (12), 3561−3566.
(60) Schiffer, M.; Edmundson, A. B. *Biophys. J.* **1967**, *7* (2), 121−135.

NEXAFS spectroscopy has confirmed the molecular orientations of alkanethiols, DPPTE, and overlying DMPC multilayers both with and without incorporated peptide on gold. Peptide presence is confirmed by bond-peak association. We have shown that the ordering of peptide-incorporated films is not diminished upon the introduction of synthetic peptide.

Acknowledgment. This work was funded by a grant from the National Science Foundation and through the NIH Biotechnology Traineeship Program. Gold substrates were prepared by Dr. Soojin Oh (UNC Chapel Hill), Dr. C. Richard Guarnieri (NC State University), and Dr. Vitalii Silin (NIST). EIS experiments were performed in Dr. Peter Fedkiw's laboratory (N.C. State University), and NEXAFS experiments were conducted at The National Synchrotron Light Source (Brookhaven National Labs) in collaboration with Dr. Kirill Efimenko (NC State University) and Dr. Zugen Fu (BNL). Special thanks go out to Melanie Chin, Thomas Lerch, Brian Pridgen, and Michael Marks (all from NC State University) for their valued assistance on this project.

LA051104W